Facile Fabrication of Co–Doped Porous Carbon from Coal Hydrogasification Semi-Coke for Efficient Microwave Absorption

Yan-Fang Li *, Li-Fang Wang, Shu-juan Gao, Tan-Lai Yu, Qi-Feng Li, Junwei Wang *

Posted Date: 9 September 2024

doi: 10.20944/preprints202409.0566.v1

Keywords: Co/C composites; microwave absorption; dielectric loss; magnetic loss

Article

Facile Fabrication of Co–Doped Porous Carbon from Coal Hydrogasification Semi-Coke for Efficient Microwave Absorption

Yan-Fang Li [1,2,*], Li-Fang Wang [1], Shu-juan Gao [1,2], Tan-Lai Yu [1,2], Qi-Feng Li [3] and Jun-Wei Wang [3,*]

[1] Department of Chemical and Materials Engineering, Lyuliang University, Lvliang Shanxi 033001, China; lllswlf@163.com (L.-F.W.); shujuangao@llu.edu.cn (S.-J.G.); 20171017@llu.edu.cn (T.-L.Y.)

[2] Institute of New Carbon-based Materials and Zero-carbon and Negative-carbon Technology, Lyuliang University, Lvliang Shanxi 033001, China;

[3] Institute of Coal Chemistry, Chinese Academy of Sciences, Taiyuan Shanxi 033000, China; liqf@sxicc.ac.cn (Q.-F.L.)

* Correspondence: liyanfang@llu.edu.cn (L.-Y.F.); wangjw@sxicc.ac.cn (J.-W.W.)

Abstract: A Co–doped porous carbon was successfully fabricated by a facile carbonizing procedure using coal hydrogasification semi-coke (SC) as the carbon and cobalt nitrate as the magnetic precursors, respectively. The microwave absorption (MA) performances were regulated by adjusting the mass ratio of the precursors. The dielectric loss from the carbon framework, the magnetic loss from nano–sized Co particles coupled with multiple scattering from the residual pores synergistically contribute to the favorable MA capabilities. When the initial mass ratio of cobalt nitrate and SC was 1:1, the Co/C composite showed the lowest reflection loss of –33.45 dB at the thickness of 4.0 mm. The effective absorbing bandwidth (EAB) could achieve 3.5 GHz at 2 mm in thickness. This work not only exploits a new avenue for the structural design and facile fabrication of dielectric and magnetic loss combinations, but also opens up another way for the high value–added utilization of SC.

Keywords: Co/C composites; microwave absorption; dielectric loss; magnetic loss

1. Introduction

With the increasing development of electronic and communication devices in recent years, more and more serious electromagnetic (EM) interference and pollution have caused great threats to the reliability of sensitive electronic devices, information security and the health of human beings. Microwave absorbing materials (MAMs) are an effective candidate to solve these issues by converting the incident EM wave to heat or other forms of energy and dissipating it [1-4].

In general, an ideal MAM should possess two significant characteristics: well-matched impedance and favorable attenuation constant. The better impedance matching means that more incident EM can enter the interior of an absorber and be dissipated, and the higher attenuation constant signify stronger microwave dissipation capabilities. Hence, the purpose of high-performance absorbers is to improve impedance matching and increase microwave attenuation capabilities simultaneously. There are two main attenuation mechanisms include dielectric loss and magnetic loss [5, 6]. Currently, carbon-based materials, as a main dielectric loss type MAMs, have become an ideal candidate due to their outstanding advantages of being light-weight, having high absorption efficiency, and having an adjustable microstructure. Typically, those cost-effective, affordable, and resource-rich carbon-based MAMs, such as biomass-based or other carbonaceous residues, have attracted widespread concern [7-9]. Wu et al. prepared a variety of biomass-based absorbers using a one-step carbonization process. The obtained spinach-derived absorbers exhibited a maximum reflection loss (RL_{min}) of −62.2 dB and a broad effective absorption bandwidth (EAB) of 7.3 GHz [10]. Our previous work used coal hydrogasification semi-coke (SC) and GO as the precursors to fabricate the absorbers by a calcination method. The composite exhibited good MA

 doi:10.20944/preprints202409.0566.v1

performance, with an EAB of 4.3 GHz and an RL_{min} of -48.8 dB at a thickness of 2.5 mm [11]. Whereas, the carbon materials only endow the absorbers with dielectric loss, which is disadvantageous to the impedance matching. Previous reports have confirmed that an effective way to get favorable MA capabilities is to combine dielectric and magnetic loss materials (Fe, Co, Ni, and their oxides) [12, 13]. This approach can not only utilize the benign magnetic loss capability of the magnetic components but also facilitate the practical applications limited by their high density [14-16].

There are multifold ways to combine the carbon materials and magnetic materials such as the sol-gel method [17], template strategy [18, 19], Metal organic framework (MOF) [20-23], carbon reduction treatment [24] or the combination of these approaches, etc [25]. For instance, Li et al. successfully prepared the tremella-like assemblies of hierarchically porous nickel cobalt/carbon (NiCo/C) by a microwave-assisted and followed sintering process. The obtained composite displayed a RLmin value of −41.6 dB with a mass ratio of 12.5 % [26]. Wu et al. prepared Co/C crabapples via a solvothermal reaction coupled with a following carbon reduction treatment. The composite exhibited a broad bandwidth of 5.9 GHz at an ultrathin thickness of 1.4 mm when the filling content was 50 wt% [27]. Fabrication of MOF is another efficient path for high-performance absorbers. They can be prepared through the reaction of metal ions and organic ligands via adding other high dielectric materials or not. Huang et al. prepared the MOF-based absorbers through a static reaction and heat treatment process using cobalt nitrate hexahydrate and 2-Methyl imidazole in the presence of luffa sponge carbon. The composites showed a RL_{min} of –60.81 dB and an EAB of 5.56 GHz at a very thin thickness of 1.68 mm [28]. Wang et al. fabricated a rod-like porous Co/C composite by directly carbonizing a Co-based MOF-74 precursor. The composite showed a RL_{min} of −38.46 dB with a coating thickness of 2.5 mm [29]. In a word, the preparation method should be directed towards simplicity, efficiency, and sustainability.

In this work, we selected SC and cobalt nitrate hexahydrate as the carbon and magnetic precursors. SC, as the residue of coal hydrogasification, exhibits several outstanding characteristics, such as high carbon content, preferable graphitization, special pore structure, and abundant sources [30]. SC has been widely applied in the fields of organic pollutants adsorber [31], further hydrogasification for methane [32, 33] or microwave absorbers [34, 35]. Using SC as a carbon source can utilize its excellent dielectric properties, environmental friendliness, and repurposing in the meanwhile. A facile preparation method is adopted via a one-step calcination process, which can largely simplify the production process and shorten the time. The obtained Co/C composites inherited superb dielectric loss capability from SC and magnetic loss from Co particles. In addition, Co particles distributed on the walls and interior of the pores could greatly enhance the interfacial polarization. The 1:1 initial mass ratio of cobalt nitrate hexahydrate and SC showed the best microwave absorption performance with a RL_{min} of –33.45 dB and an EAB of 3.47 GHz at 2.0 mm in thickness, making the porous Co/C composites a promising candidate for MAMs.

2. Results and Discussion

2.1. Morphology and Structure

Figure 1 shows the schematic synthesis process of Co-embedded porous carbon composites.

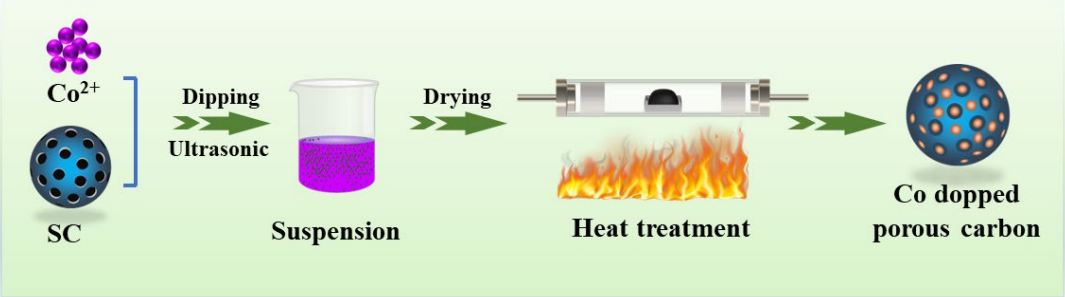

Figure 1. Schematic illustration of the synthesis process of Co-embedded porous carbon composites.

 doi:10.20944/preprints202409.0566.v1

The X-ray diffraction technique was used to verify the crystalline and phase composition of SC and Co/C composites. As shown in Figure 2(a), different proportions of precursors have no obvious influence on the composition of Co/C composites, reflecting nearly the same peaks on the patterns. Specifically, all the Co/C samples have three strong diffraction peaks located at 44.3°, 51.6°, 75.9°, which can be indexed to the (111), (200) and (220) planes of face-centered cubic cobalt (JCPDS No. 15-0806), respectively. The results confirm the in-situ reduction of Co^{2+} to Co metal during the calcination process. The sharp peak of SC pattern located at 26.6° responds to the graphitized crystal plane (002) of carbon, indicating that SC has certain graphitized carbon domains. Whereas, the diffraction peak of Co/C composites at 26.6° becomes much fainter compared with SC, which is the direct evidence of reaction between SC and cobalt nitrate hexahydrate in the pyrolysis process. Particularly, there also appear other peaks except for 26.6° and 44.6°. This is consistent with our previous research results that SC not only contains C but also includes other elements such as O, N, Fe, Mn, Ni, etc. These components are the source of other peaks [11]. The existence of these elements also contributes to dipole and interface polarization, which is conducive to the enhancement of microwave absorption.

Raman spectroscopy was further used to investigate the effect of cobalt salt on the carbon graphitization degree during the carbonization process, as illustrated in Figure 2(b). There are two characteristic peaks in each sample, which are roughly at 1350 cm^{-1} (D-band) and 1580 cm^{-1} (G-band). The local defect and the disordered carbon are represented by the D-band, whereas the graphited C atoms observed for sp^2 carbon domains are represented by the G-band. The peak intensity of D-band to G-band (I_D/I_G) is usually used to evaluate the degree of graphitization of carbon-based materials [36, 37]. As shown in Figure 2(b), the Co/C composites exhibit a much higher I_D/I_G than that of SC (0.83). Since cobalt salt could catalyze the graphitization of carbon, the increased I_D/I_G value could be attributed to the transitional stage from amorphous carbon to nanocrystalline graphite according to the phenomenological three-stage model proposed by Ferrari and Roberston [38]. Due to the nano size of crystalline graphite, the I_D/I_G values show a decline tendency. In addition, the higher the content of the cobalt salt precursor, the higher the I_D/I_G value. Specifically, the I_D/I_G value rises from 0.95 to 0.97 for Co/C-0.75 and Co/C-2. The enhancement of nanocrystalline graphite would promote conductivity and polarization capability, which is in favor of conductive loss and polarization loss for better microwave absorption.

Thermogravimetric analysis (TGA) was carried out to determine the accurate content of Co nanoparticles in Co/SC composites. Figure 2(c) displays the thermogravimetric curves of Co/C composites in air atmosphere. The samples were heated to 100 °C and kept for 30 min for the removal of adsorbed water. The samples were kept for 4 h at 700 °C then for the sufficient redox reaction. The weight fluctuation of the samples mainly originated from the oxidation of Co nanoparticles to Co_3O_4, the combustion of carbon to CO_2 or other carbon oxides and the splitting of other components such as O, N. The weight increase from 100 °C to ~440 °C is mainly attributed to the oxidation of Co to Co_3O_4 while the sharp decline from ~440 °C to ~580 °C are primarily ascribed to carbon consumption. The weight percentage was finally constant at 42.83 %, 47.39 %, 53.57 % and 59.87 %, respectively. The content of Co in the Co/C composites can be evaluated via the following formula:

$$\mathrm{wt\%_{Co}} = \frac{3 * M(\mathrm{Co}) * R}{M(\mathrm{Co_3O_4})}$$

where $\mathrm{wt\%_{Co}}$ represents the content of Co in the Co/C composites, R stands for the residual weight percentage after the reaction. *M*(Co) and *M*(Co_3O_4) represent the molecular weights of Co and Co_3O_4 respectively [39]. Hence, the content of Co nanoparticles in Co/C-0.75, Co/C-1, Co/C-1.5 and Co/C-2 composites was determined to be 31.48 wt%, 34.83 wt%, 39.37 wt% and 44.00 wt%, respectively. The above results illustrate that the Co content in Co/C composites has positive correlation with the doping of cobalt salt.

The chemical state information on the surface of the samples was characterized by XPS. Figure 2(d) shows the survey spectra of SC and Co/C composites. The Co/C composites show three typical peaks located at 282 eV, 529 eV and 776 eV, corresponding to C 1s, O 1s and Co 2p respectively, which demonstrate the existence of C, O and Co elements in Co/C composites. The high-resolution C 1s XPS

 doi:10.20944/preprints202409.0566.v1

spectrum (Figure 2e) of Co/C-1 consists of three deconvoluted peaks at 284.8 eV, 286.4 eV, 288.9 eV, corresponding to C–C/C=C, C–O and C=C functional groups respectively. Four different Co species types are visible in the high-resolution Co 2p XPS spectra. The peaks at 780.8 eV and 795.6 eV correspond to Co $2p_{3/2}$ and Co $2p_{1/2}$ respectively, while the peaks at 784.8 eV and 803.3 eV are the satellite peaks of Co 2p from Co metal. The results are consistent with the analysis of XRD that Co metal is the main existence state [38].

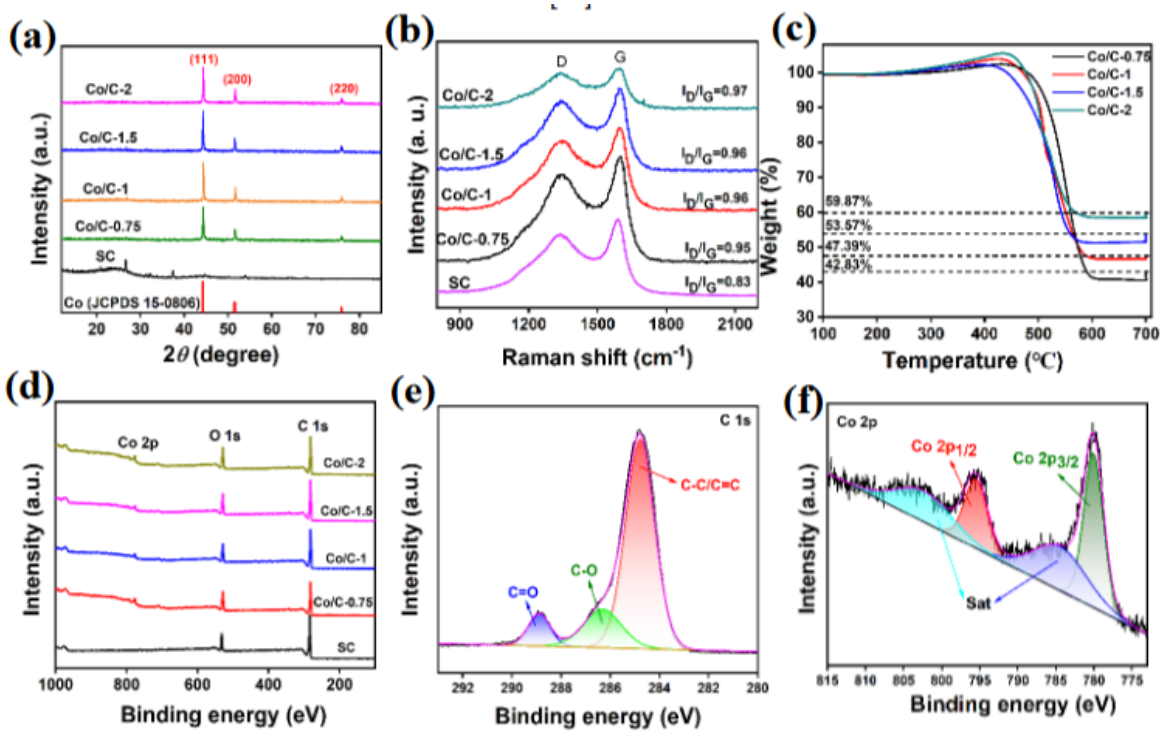

Figure 2. XRD patterns (a) and Raman spectra (b) of SC and Co/C composites; TGA curves for Co/C composites. XPS survey spectra of the samples (d) and the high-resolution spectrum of C1s (e), N1s and Co2p (f) for Co/C-1.

The magnetic properties of all the samples were measured at 300 K. As shown in Figure 3, all the Co/C composites exhibit typical ferromagnetic characteristics with magnetic hysteresis loops. Co/C composites have considerably superior magnetic characteristics than that of SC (Figure S2), suggesting that magnetic elements were successfully incorporated during the carbonization process. The saturation magnetization (Ms) values of the Co/C composite increase with the elevated Co doping, which is consistent with the TGA results for increased Co content from Co/C-0.75 to Co/C-2. Specifically, the Ms values of Co/C-0.75, Co/C-1, Co/C-1.5 and Co/C-2 are 34.93 emu/g, 40.83 emu/g, 45.78 emu/g and 56.44 emu/g respectively. Noteworthy, Co/C-1 displays the highest coercive forces (Hc, 138 Oe) than those of other Co/C composites, which is attributed to its peculiar microstructure for shape anisotropy. The results demonstrate that these Co/C composites with various morphology and dimension possess tailorable intrinsic dielectric properties and magnetic response abilities.

 doi:10.20944/preprints202409.0566.v1

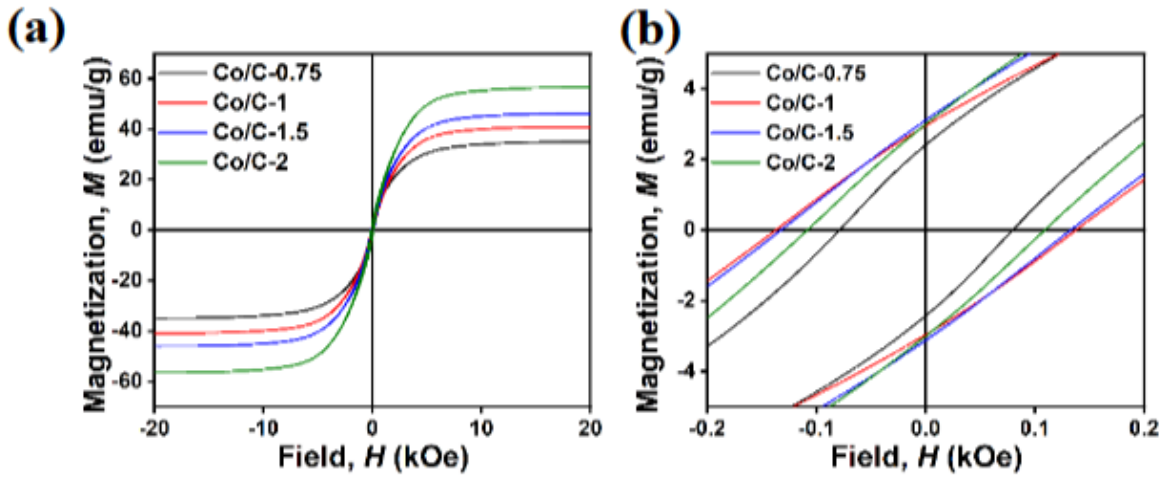

Figure 3. VSM hysteresis loop (a) and the magnification image of Co/C composites (b).

The morphologies and structures were characterized by SEM, as shown in Figure 4. The composites inherited plenty of pores from SC (Figure S1). Abundant spherical, quasi-spherical and irregular Co particles distribute in the pores and walls of SC, resulting in a sharp decrease of the pores compared with SC. Different Co doping has a significant effect on the size and distribution of Co nanoparticles. The size and distribution of Co particles were measured via the Nano measurer software from the SEM images. Co/C-2 possesses the biggest Co mean size of ~150 nm and the widest distribution. In contrast, the mean size of Co/C-1 and Co/C-1.5 is relatively small at ~100 nm and ~60 nm respectively. Remarkably, Co/C-1 shows a wider distribution than other Co/C composites, combined with its dynamic spherical, quasi-spherical and irregular shapes, contributing to a better shape anisotropy. The results illustrate that the precursors would participate in the reaction process, thus influencing the growth of grains, dynamic sizes and distributions. According to our previous analysis, possible reactions in the annealing process are listed as follows:

$$Co(NO_3)_3 + C \rightarrow Co + CO_2 + NO_2 \quad (1)$$

$$Co(NO_3)_3 \rightarrow Co_3O_4 + NO_2 + O_2 \quad (2)$$

$$C + O_2 \rightarrow CO_2 \quad (3)$$

$$CO_2 + C \rightarrow 2CO \quad (4)$$

$$Co_3O_4 + C\,(\text{or}\,CO) \rightarrow Co + CO_2 \quad (5)$$

The EDS mapping of Co/C-1 composites was performed to observe the elemental distribution. As shown in Figure 4(i), Co, O, and C atoms uniformly distribute in the composites, indicating that the Co nanoparticles embedded in porous carbon composites were successfully fabricated.

 doi:10.20944/preprints202409.0566.v1

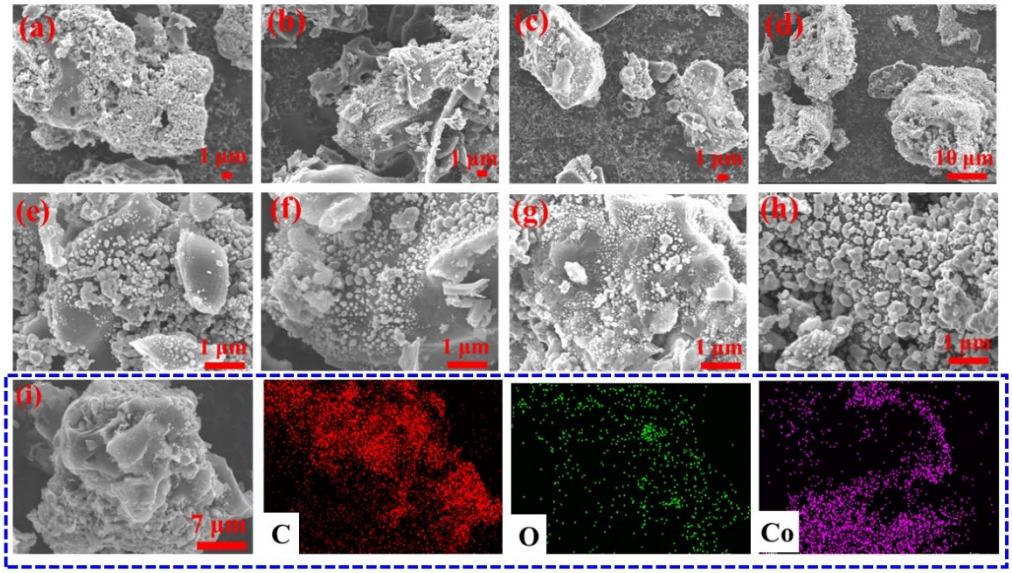

Figure 4. The SEM images of the Co/C-0.75 (a, e), Co/C-1 (b, f), Co/C-1.5 (c, g) and Co/C-2(d, h). The element mapping analysis of Co/C-1 (i).

3.2. Microwave Absorption Performance

The EM absorption performance of the as-prepared composites was studied through the calculated RL value according to the following equations:

$$\mathrm{RL(dB)} = 20\log\left|\frac{Z_{\mathrm{in}} - Z_0}{Z_{\mathrm{in}} + Z_0}\right| \quad (1)$$

$$Z_{\mathrm{in}} = Z_0\left(\mu_{\mathrm{r}}/\varepsilon_{\mathrm{r}}\right)^{0.5}\tanh\left(2\pi jfd/c\sqrt{\mu_{\mathrm{r}}\varepsilon_{\mathrm{r}}}\right) \quad (2)$$

where Z_0 is the air impedance, Z_{in} is the input impedance, d is the thickness of the absorbers, f represents the microwave frequency and c is the velocity of light in free space. ε_{r} and μ_{r} stand for the complex permittivity and complex permeability, respectively. The RL value below –10 dB is regarded as an effective microwave absorption, which mean more than 90% of the electromagnetic energy can be attenuated, and the corresponding frequency range is called the effective absorption bandwidth (EAB). The RL curves and the 3D plots of SC and Co/C composites in the range of 2–18 GHz are displayed in Figure 5. As shown in Figure 5，all the Co/C composites show an enhanced MA compared with SC, demonstrating that the Co incorporation has a significant effect on the composition, structure, and electromagnetic parameters, which endows the composites with improved MA performance. The $\mathrm{RL_{min}}$ of SC is far below –10 dB at the calculated matching thicknesses. Although Co/C-0.75 has the strongest absorbing ability with the $\mathrm{RL_{min}}$ value of –38.33 dB, the matching thickness is as high as 5.0 mm, which is disadvantageous for practical applications. Co/C-1exhibits the moderate $\mathrm{RL_{min}}$ of –33.45 dB at a thickness of 4.0 mm. The EAB of Co/C-1 is 3.47 GHz (10.15–13.62 GHz) at 2.0 mm in thickness. The $\mathrm{RL_{min}}$ of Co/C-1.5 and Co/C-2 show a declining tendency compared with Co/C-1, which indicates that different compositions, sizes and microstructures of Co/C composites would influence the electromagnetic parameters and thus diverse MA performances.

Preprints.org (www.preprints.org) | NOT PEER-REVIEWED | Posted: 9 September 2024 doi:10.20944/preprints202409.0566.v1

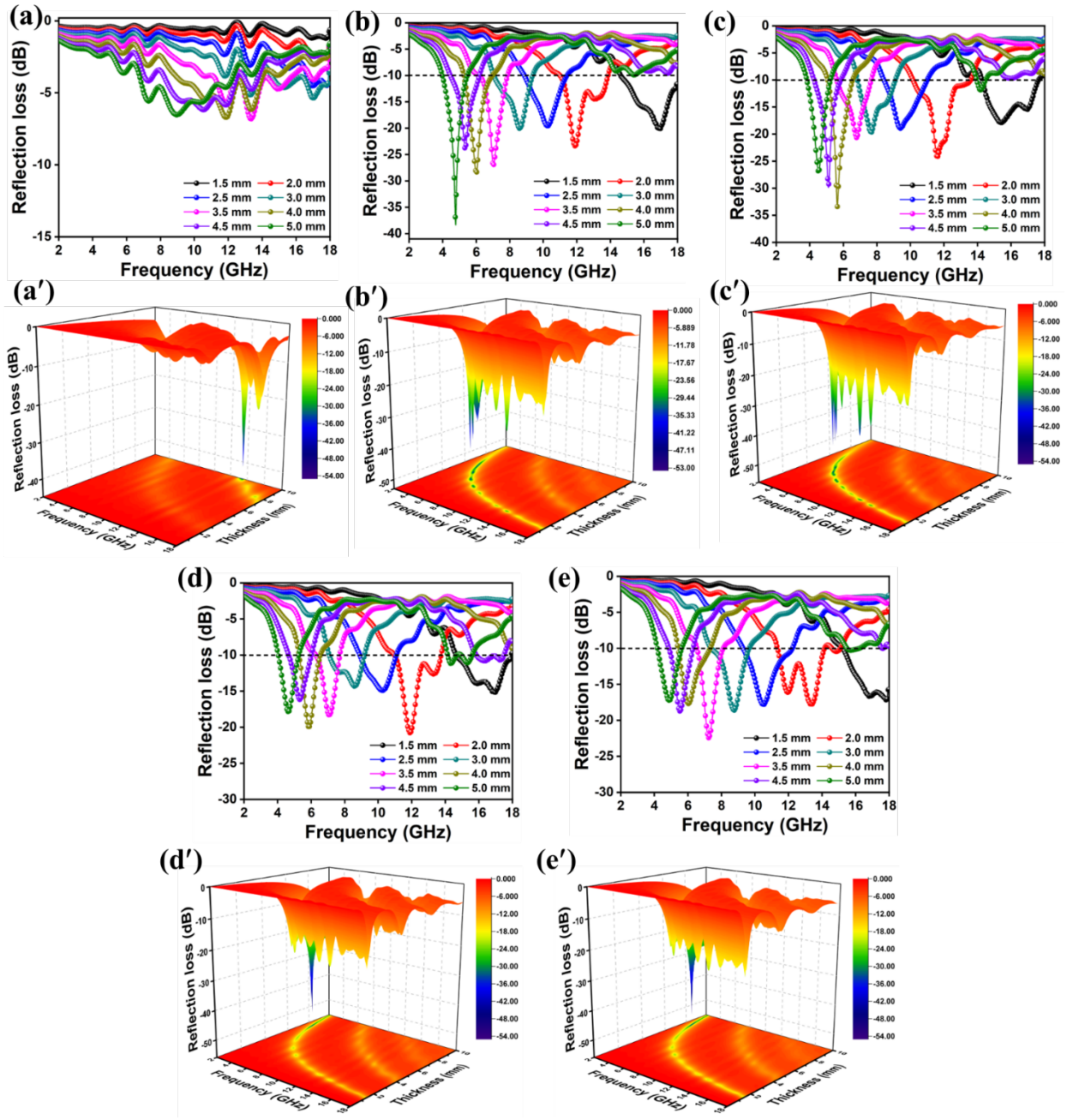

Figure 5. Calculated RL curves and 3D plots of SC (a, a′), Co/C-0.75 (b, b′), Co/C-1 (c, c′), Co/C-1.5 (d, d′) and Co/C-2 (e, e′).

The complex permittivity ($\varepsilon_r = \varepsilon' - j\varepsilon''$) and permeability ($\mu_r = \mu' - j\mu''$) are the primarily determinants for the EM properties. ε′ and μ′ denote the ability to store electric and magnetic energies respectively, while ε″ and μ″ represent the ability to dissipate the electric and magnetic energies respectively. To further investigate the relationship between the complex permittivity, complex permeability and the MA performances, the frequency dependences of permittivity and permeability are depicted, as shown in Figure 6. In Figure 6(a), all the samples display a downward tendency with the increased frequency, which can be attributed to dielectric polarization relaxation behavior of Co/C -paraffin hybrids. The ε′ and ε″ values of SC fluctuate from 3.74 to 3.45 and 0.65 to 0.35 respectively, which are much lower than those of Co/C composites. This is attributed to the fact that SC has the inferior storage capability of electric field, indicating that the electrical conductivity and graphitization are not satisfactory. The electric storage and dissipation abilities are attributed to carbon and Co for Co/C composites. Among the Co/C composites, Co/C-1 exhibits outstanding

 doi:10.20944/preprints202409.0566.v1

electric storage and attenuation capabilities, which is mainly ascribed to its peculiar microstructure. Although the graphitization degree of Co/C-1 is moderate, the variform Co nanoparticles and the resulting abundant pores made more prominent contribution to the conductivity and polarization capabilities than its counterparts, bringing about higher ε′ (12.08–10.49) and ε″ (3.44–2.90). Whereas, more and bigger Co particles would restrict the polarization of dipoles for better electric storage capability, thus exhibit a decrease for Co/C-2. The incorporation of magnetic Co nanoparticles greatly enhanced the magnetic storage and attenuation capabilities, showing much higher μ′ and μ″ for the Co/C composites compared with SC. Noteworthy, Co/C-1 exhibits the lowest μ′ and μ″, this could be ascribed to its highest Hc, as shown in the previous VSM analysis. A high Hc mean more difficult magnetizability for magnetic energies storage and dissipation capabilities, resulting in the lowest μ′ and μ″ for Co/C-1. In addition, dielectric loss and magnetic loss tangent ($\tan\delta_\varepsilon = \varepsilon''/\varepsilon'$, $\tan\delta_\mu = \mu''/\mu'$) are crucial parameters to determine the dominant loss mechanism in the MA mechanism. As shown in Figure 6 (c) and (f), dielectric loss is the main contribution to the MA performance of Co/C-1 because the tanδε value (above 0.24) are larger than the tanδμ values (below 0.2) in almost the entire frequency ranges, demonstrating that the dielectric loss is the dominant loss mechanism for the attenuation of electromagnetic waves [40].

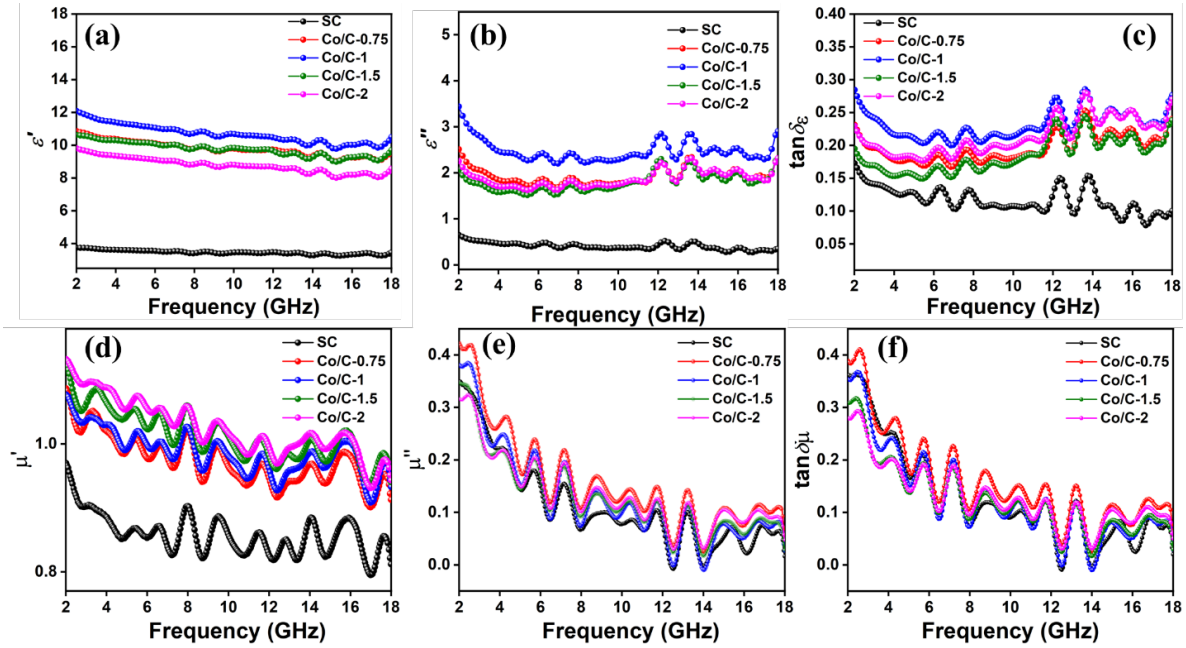

Figure 6. Real (a) and imaginary (b) permittivity, real (c) and imaginary (d) permeability, dielectric (e) and magnetic (f) loss tangent of the composites.

To further investigate the existence of dielectric polarization and the related relaxation, the relationship between ε′ and ε″ was analyzed based on the Debye relaxation theory:

$$(\varepsilon' - \frac{\varepsilon_s + \varepsilon_\infty}{2})^2 + (\varepsilon'')^2 = (\frac{\varepsilon_s - \varepsilon_\infty}{2})^2$$

In the curve of ε′~ε″, an approximate semicircle (Cole-Cole semicircle) represents one Debye relaxation process. The polarization in the tested frequency range mainly includes interfacial polarization and dipolar polarization. The Cole-Cole plots are shown in Figure 7. As shown in Figure 7(a)-(e), Co/C composites exhibit more semicircles compared with SC, which is attributed to the introduction of multiple nano-heterointerfaces due to the incorporation of Co nanoparticles and Co embedding into the pores of SC. Specifically, SC shows five distinct semicircles, while the Co/C composites exhibit seven distinct semicircles except Co/C-2. Remarkably, Co/C-2 exhibits six distinct semicircles and a longer tail than other Co/C composites. The tail is the symbol of conductive loss ,suggesting that Co/C-2 possess stronger conductive ability [41].

 doi:10.20944/preprints202409.0566.v1

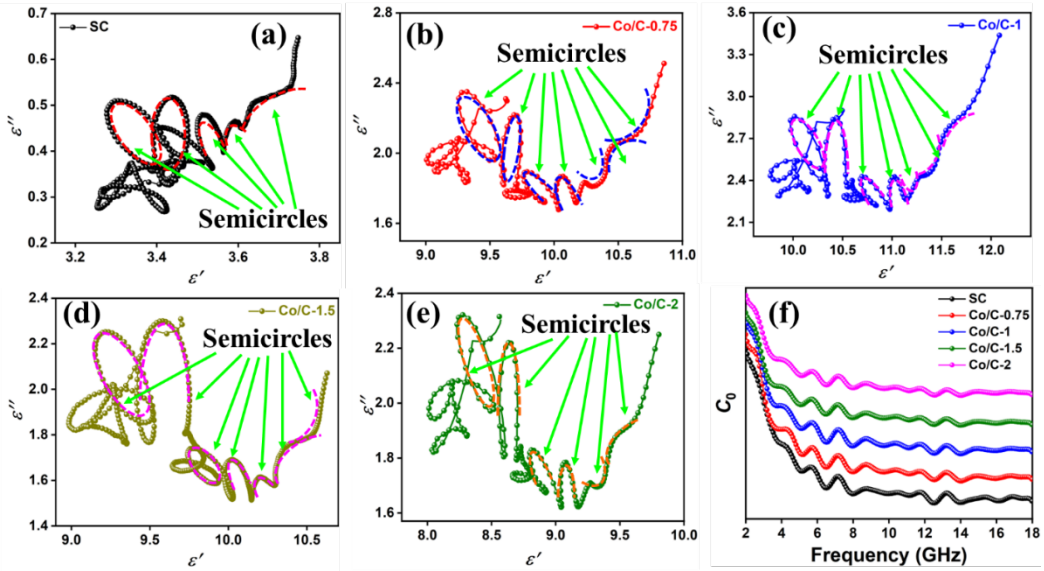

Figure 7. Cole–Cole diagrams for the paraffin composites (a-e) and the the C_0-f curves of the composites (f).

The magnetic loss mechanism was analyzed. The following formula is usually used to analyze the eddy current effect on the EM absorbing performance:

$$C_0 = \mu''(\mu')^{-2} f^{-1}$$

If C_0 is constant in the curve of C_0-f, the eddy current loss is considerable. As shown in Figure 7(f), C_0 almost fluctuates in the whole tested frequency. The C_0 value falls dramatically with increasing frequency below 8 GHz and then continuously changes in 8–18 GHz. Therefore, eddy current loss is not the dominant magnetic loss mechanism in 2–18 GHz. Natural resonance is represented by the fluctuating peaks at lower frequencies, whereas exchange resonance is represented by the peaks at higher frequencies.

To further investigate the influence of impedance matching and microwave attenuation capability on the MA performances, the calculated attenuation constant (α) and impedance matching are shown in Figure 8. The higher α value means stronger attenuation capability of an absorber to dissipate the EM energies. If the input impedance of an absorber is equal to that of the free space, the value of $|Z_{in}/Z_0|$ is 1. The closer of $|Z_{in}/Z_0|$ value to 1 means more input EM waves would enter the interior of an absorber and be dissipated. A high α and benign impedance matching capability are two prominent factors for favorable MA performances. As shown in Figure 8, SC exhibits the lowest α compared with Co/C composites, indicating the weakest EM attenuation capability, meanwhile, the value of $|Z_{in}/Z_0|$ is far less than 1, which manifests the inferior impedance matching performance. Among the Co/C composites, Co/C-1 exhibits the highest α and the best impedance matching abilities, which is the prerequisite for favorable MA performance. The results are consistent with the calculated RL results.

 doi:10.20944/preprints202409.0566.v1

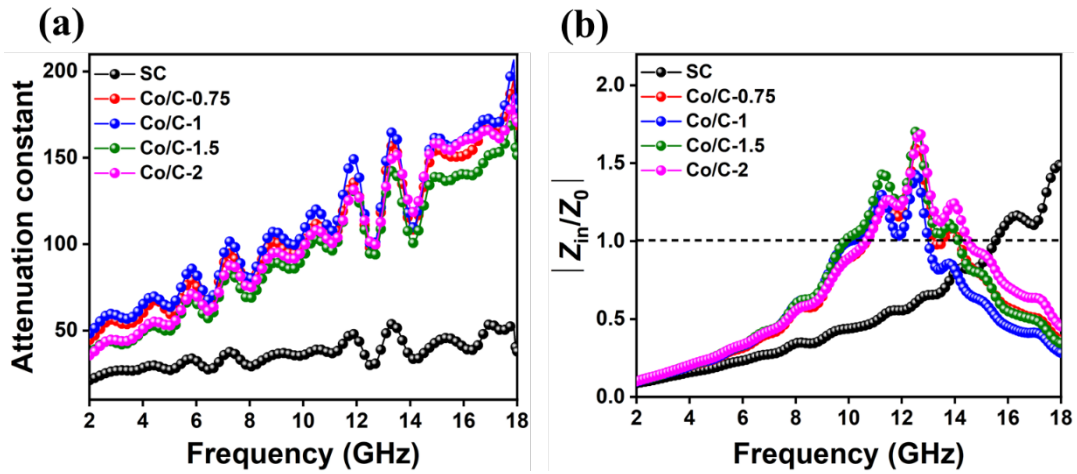

Figure 8. The attenuation constant (a) and impedance matching at 2.0 mm in thickness (b) curves of the composites.

3.3. Microwave Absorption Mechanism

The microwave absorption mechanism of those Co/C composites is illustrated in Figure 9. First, the composites not only inherited several defects and residual groups (C=O, C–O) from SC, but also received many defects due to the presence of Co, which would act as the polarization centers and contribute to dipole polarization loss. The fabrication process of the composites also brought about plentiful heterogeneous interfaces (Co/C, Co/air, and C/air), which is conducive to interfacial polarization loss for favorable MA performances; Secondly, the graphited carbon and Co nanoparticles provide suitable local conductivity, which brings high conductive loss. Third, because of the significant shape anisotropy, the nano-sized Co in the composites increases the magnetic losses by promoting the formation of exchange resonance and domain wall resonance in magnetic entities. In addition, the residual pores from SC could prolong the EM wave transmission path in the composites through multiple scattering, which is beneficial for the conversion of EM wave energy to other sorts of energies. The pores are also helpful for impedance matching. The synergistic effects of the above-mentioned factors jointly contribute to overall high-performance MA.

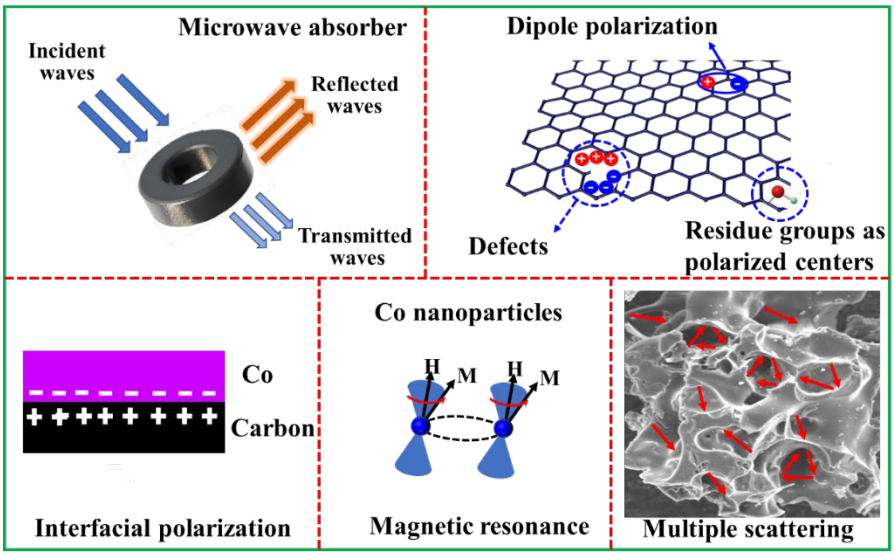

Figure 9. Schematic illustration of the microwave absorption mechanism.

3. Materials and Methods

3.1. Materials

 doi:10.20944/preprints202409.0566.v1

SC, acquired from the Institute of Coal Chemistry, was pulverized and passed through a 140-mesh screen. Cobalt nitrate hexahydrate ($Co(NO_3)_2 \cdot 6H_2O$) was obtained from Shanghai Aladdin biochemical technology Co., Ltd. Deionized water (DI) was homemade in our lab. SC was dried at 80 ℃ before use.

3.2. Preparation of Hierarchical Porous Co/C Absorbers

Co-embedded porous carbon was prepared via a facile impregnation coupled with a following calcination strategy. After dissolving $Co(NO_3)_2 \cdot 6H_2O$ in deionized water, a certain amount of SC was added to the solution of $Co(NO_3)_2 \cdot 6H_2O$. The suspension was sonicated for 30 min and kept overnight. The mixture was then stirred through a magnetic heated stirrer, and dried in a vacuum oven until the solvent was completely evaporated. The absorbers were prepared by calcinating the above precursor hybrids at 700 °C for 2 h in N_2 atomosphere. The absorbers with different initial $Co(NO_3)_2 \cdot 6H_2O$ and SC mass ratio of 0.75:1, 1:1, 1.5:1 and 2:1 were marked as Co/C-0.75, Co/C-1, Co/C-1.5 and Co/C-2, respectively.

3.3. Characterization

X-ray powder diffraction (XRD, Bruker Advance D8) was used to characterize the crystallization of the absorbers utilizing Cu Kα (λ=1.5406 Å) at 40 mA and 40 kV in the 2θ range of 10°-90°. The surface morphologies and elemental mapping distributions were examined using scanning electron microscopy (SEM, JEOL JSM-7001) and energy dispersive spectroscopy (EDS, X Flash 5010), respectively. Using a 532 nm laser beam as the light source, Raman spectroscopy (Thermo Fisher Scientific, Dxr2xi) was used to record Raman spectra. Utilizing Al Kα (1486.6 eV) as the monochromatic source, X-ray photoelectron spectroscopy (XPS, ESCALAB 250Xi) was used to describe the chemical states of the produced hybrids. The magnetic hysteresis loops were measured using a vibrating sample magnetometer (VSM, LakeShore7404) at room temperature. The thermogravimetric analysis was carried out using a thermal analyzer (TGA-50, Shimadzu) in an air atmosphere. The samples were heated to 100 °C with a heating rate of 10 °C/min and kept for 30 min, and then heated continually to 700 °C and kept for 4 h.

The coaxial-line approach was utilized to assess the complex permittivity and permeability between 2 GHz and 18 GHz with a vector network analyzer (VNA, E5071C).The measured composites and paraffin were uniformly mixed in a mass ratio of 6:4 and shaped into a ring with a toroidal shape (Φ_{out} :7.00 mm, Φ_{in} : 3.04 mm). According to the transmission theory, the reflection loss, the attenuation constant, and the impedance matching were determined.

4. Conclusions

In summary, a magnetic Co embedded heterostructure in coal-derived carbon framework is successfully prepared by a facile and cost-effective thermal annealing method. The composition, morphology, size, and graphitization were adjusted via the initial mass ratio of the carbon and magnetic precursors. Graphited carbon, nano-sized Co, residual groups, and their synergistic effects on dipole and interfacial polarization, conductivity loss, magnetic loss, and multiple scattering lead to excellent MA performances. The results show that when the thickness is 4.0 mm, the RL_{min} is as low as −33.45 dB, and the effective absorption bandwidth is 3.47 GHz at 2.0 mm in thickness. This work not only provides a facile strategy for the fabrication of highly efficient absorbers, but also opens up a new opportunity for the high value-added utilization of SC. This strategy could also extend to other cost-effective coal–based or biomass–based carbon materials.

Supplementary Materials: The following supporting information can be downloaded at www.mdpi.com/xxx/s1: Figure S1: The SEM images of SC.; Figure S2: Magnetic hysteresis loops of SC.

Author Contributions: Conceptualization, Y.-F.L.; investigation, S.-J.G. and Q.-F.L.; methodology, Y.-F.L. and J.-W.W.; validation, L.-F.W. and T.-L.Y.; writing—original draft, Y.-F.L.; writing—review & editing, Y.-F.L. All authors have read and agreed to the published version of the manuscript.

 doi:10.20944/preprints202409.0566.v1

Funding: This work was supported by Natural Science Foundation of Shanxi Province (202303021222253).

Data Availability Statement: Data are contained within the article and supplementary materials.

Conflicts of Interest: The authors declare no conflicts of interest.

References

1. Guan, H.; Wang, Q.; Wu, X.; Pang, J.; Jiang, Z.; Chen, G.; Dong, C.; Wang, L.; Gong, C., Biomass derived porous carbon (BPC) and their composites as lightweight and efficient microwave absorption materials. *Compos. Pt. B-Eng.* **2021,** 207.
2. Lv, H.; Yang, Z.; Pan, H.; Wu, R., Electromagnetic absorption materials: Current progress and new frontiers. *Prog. Mater. Sci.* **2022,** 127.
3. Zhao, H.; Cheng, Y.; Liu, W.; Yang, L.; Zhang, B.; Wang, L. P.; Ji, G.; Xu, Z. J., Biomass-Derived Porous Carbon-Based Nanostructures for Microwave Absorption. *Nano-Micro Lett.* **2019,** 11, (1).
4. Zhou, M.; Gu, W.; Wang, G.; Zheng, J.; Pei, C.; Fan, F.; Ji, G., Sustainable wood-based composites for microwave absorption and electromagnetic interference shielding. *J. Mater. Chem. A* **2020,** 8, (46), 24267-24283.
5. Li, W.; Liu, Y.; Guo, F.; Du, Y.; Chen, Y., Self-assembly sandwich-like Fe, Co, or Ni nanoparticles/reduced graphene oxide composites with excellent microwave absorption performance. *Appl. Surf. Sci.* **2021,** 562.
6. Qu, Z.; Wang, Y.; Wang, W.; Yu, D., Robust magnetic and electromagnetic wave absorption performance of reduced graphene oxide loaded magnetic metal nanoparticle composites. *Adv. Powder Technol.* **2021,** 32, (1), 194-203.
7. Lu, X.; Li, X.; Zhu, W.; Xu, H., Construction of embedded heterostructures in biomass-derived carbon frameworks for enhancing electromagnetic wave absorption. *Carbon* **2022,** 191, 600-609.
8. Yang, W.; Yan, L.; Jiang, B.; Wang, P., Crumpled nitrogen-doped porous carbon nanosheets derived from petroleum pitch for high-performance and flexible electromagnetic wave absorption. *Ind. Eng. Chem. Res.* **2022,** 61, 2799−2808.
9. Wang, H.; Meng, F.; Li, J.; Li, T.; Chen, Z.; Luo, H.; Zhou, Z., Carbonized Design of Hierarchical Porous Carbon/Fe3O4@Fe Derived from Loofah Sponge to Achieve Tunable High-Performance Microwave Absorption. *ACS Sustain. Chem. Eng.* **2018,** 6, (9), 11801-11810.
10. Wu, Z.; Tian, K.; Huang, T.; Wei Hu; Xie, F., Hierarchically porous carbons derived from biomasses with excellent microwave absorption performance. *ACS Appl. Mater. Interfaces* **2018,** 10, 11108−11115.
11. Li, Y.; Li, X.; Li, Q.; Rong Zhang, Y.; uhua Zhao; Wang, J., Fabrication of flexible thermoplastic polyurethane/coal hydrogasification semi-coke composites with low rGO content for high-performance microwave absorption. *ACS Appl. Electron. Mater.* **2022,** 4, 5941−5952.
12. Zhang, D.; He, W.; Quan, G.; Wang, Y.; Su, Y.; Lei, L.; Du, Y.; Hong, Y.; Wang, S.; Tang, Y.; Zhang, W.; Chen, Y., Sterculia lychnophora seed-derived porous carbon@$CoFe_2O_4$ composites with efficient microwave absorption performance. *Appl. Surf. Sci.* **2023,** 607.
13. Zhou, C.; Wang, X.; Luo, H.; Deng, L.; Wang, S.; Wei, S.; Zheng, Y.; Jia, Q.; Liu, J., Interfacial design of sandwich-like CoFe@$Ti_3C_2T_x$ composites as high efficient microwave absorption materials. *Appl. Surf. Sci.* **2019,** 494, 540-550.
14. Wang, Y.; Zhao, P.; Liang, B.; Wan, G.-S., Carbon nanotubes decorated Co/C from ZIF-67/melamine as high efficient microwave absorbing material. *Carbon* **2023,** 202, 66-75.
15. Quan, B.; Xu, G.; Gu, W.; Sheng, J.; Ji, G., Cobalt nanoparticles embedded nitrogen-doped porous graphitized carbon composites with enhanced microwave absorption performance. *J. Colloid Interface Sci.* **2019,** 533 297–303.
16. Zhou, X.; Zhao, B.; Lv, H., Low-dimensional cobalt doped carbon composite towards wideband electromagnetic dissipation. *Nano Res.* **2023,** 16, (1), 70-79.
17. Liu, Q.; Zhang, D.; Fan, T., Electromagnetic wave absorption properties of porous carbon/Co nanocomposites. *Appl. Phys. Lett.* **2008,** 93, 013110.
18. Jing Yan, Y. H., Chen Chen, Xudong Liu, Hui Liu, The 3D CoNi alloy particles embedded in N-doped porous carbon foams for high-performance microwave absorbers. *Carbon* **2019,** 152, 545-555.
19. Wang, L.; Du, Z.; Bai, X.; Lin, Y., Constructing macroporous C/Co composites with tunable interfacial polarization toward ultra-broadband microwave absorption. *J. Colloid Interface Sci.* **2021,** 591, 76-84.
20. Wu, Q.; Wang, J.; Jin, H.; Dong, Y., Facile synthesis of Co-embedded porous spherical carbon composites derived from Co_3O_4/ZIF-8 compounds for broadband microwave absorption. *Compos. Sci. Technol.* **2020,** 195, 108206.
21. Zhang, Y.; Zhang, H.-B.; Wu, X.; Zhiming Deng, Nanolayered Cobalt@Carbon Hybrids Derived from Metal−Organic Frameworks for Microwave Absorption. *ACS Appl. Nano Mater.* **2019,** 2, 2325−2335.
22. Jin, H.; Wang, J.; Yang, S.; Wu, Q., ZIF-67-derived micron-sized cobalt-doped porous carbon-based microwave absorbers with g-C_3N_4 as template. *Ceram. Int.* **2021,** 47, 11506–11513.

23. Sun, Q.; Li, J.; Zhang, H.; He, X.; Wu, B.; Wang, J.; Mahmood, N.; Jian, X., The MOFs/COFs-derivant decorating FeSiAl coupling magnetic and electrical losses for enhanced microwave absorption. *Appl. Surf. Sci.* **2024,** 651.
24. Liang , J.; Chen, J.; Shen, H.; Ketao Hu; Binnan Zhao; Kong, J., Hollow porous bowl-like nitrogen-doped cobalt/carbon nanocomposites with enhanced electromagnetic wave absorption. *Chem. Mat.* **2021,** 33, 1789−1798.
25. Fu, M.; Yu, H.; Chen, W., Construction of Co_3O_4 porous rod/graphene heterostructures toward strong and broadband microwave absorption applications. *Appl. Surf. Sci.* **2023,** 622.
26. Li, C.; Sui, J.; Zhang, Z.; Jiang, X., Microwave-assisted synthesis of tremella-like NiCo/C composites for efficient broadband electromagnetic wave absorption at 2–40 GHz. *Chem. Eng. J.* **2019,** 375, 122017.
27. Wu, N.; Liu, C.; Xu, D.; Jiurong Liu, Ultrathin high-performance electromagnetic wave absorbers with facilely fabricated hierarchical porous Co/C crabapples. *J. Mater. Chem. C* **2019,** 7, 1659.
28. Huang, Y.; Tian, K.; Zhang, C.; Wang, J., Lightweight and efficient luffa sponge carbon/Co composites with adjustable electromagnetic wave absorption properties. *J. Colloid Interface Sci.* **2023,** 652, 1138–1147.
29. Wang, X.; Guan, Y.; Zhang, R.; Zhang, R., Facile synthesis of cobalt nanoparticles embedded in a rod-like porous carbon matrix with excellent electromagnetic wave absorption performance. *Ceram. Int.* **2021,** 47, 643–653.
30. Li, Y.; Li, X.; Kang, M.; Zhao, Y.; Li, Q.; Wang, J., Fabrication of flexible waterborne polyurethane/Fe-doped residual carbon from coal hydrogasification semi-coke composites for high-performance microwave absorption. *Compos. Pt. A-Appl. Sci. Manuf.* **2023,** 174.
31. Li, P.; Ailijiang, N.; Cao, X.; Lei, T.; Liang, P.; Zhang, X.; Huang, X.; Teng, J., Pretreatment of coal gasification wastewater by adsorption using activated carbons and activated coke. *Colloid Surf. A-Physicochem. Eng. Asp.* **2015,** 482, 177-183.
32. Ding, X.; Zhang, Y.; Zhang, T.; Tang, J.; Xu, Y.; Zhang, J., Effect of Operational Variables on the Hydrogasification of Inner Mongolian Lignite Semicoke. *Energy Fuels* **2013,** 27, (8), 4589-4597.
33. Ding, X. K.; Zhang, T. K.; Zhang, Y. F.; Xu, Y.; Zhang, G. J., Hydrogasification of Low-Oxygen Semi-Coke to Produce Methane by Consuming Less Hydrogen. *Appl. Mech. Mater.* **2013,** 316-317, 124-127.
34. Gao, F.; Li, Y.; Mao, L.; Wang, Y.; Zhu, B.; Liang, L.; Li, G.; Zhang, R., Facile synthesis of Co/SC microwave absorbents by recycling coal hydrogasification residue. *Mater. Lett.* **2022,** 308.
35. Gao, S.; Chen, L.; Zhang, Y.; Shan, J., Fe nanoparticles decorated in residual carbon from coal gasification fine slag as an ultra-thin wideband microwave absorber. *Compos. Sci. Technol.* **2021,** 213.
36. Ferrari, A.; Robertson, J., Interpretation of Raman spectra of disordered and amorphous carbon. *Phys. Rev. B* **2000,** 61, (20), 14095.
37. Deng, X.; Gao, S.; Liu, Y.; Bao, Y.; Zhu, Y.; Fu, Y., Cellular-like sericin-derived carbon decorated reduced graphene oxide for tunable microwave absorption. *Appl. Surf. Sci.* **2022,** 599.
38. Cui, J.; Wang, X.; Huang, L., Environmentally friendly bark-derived Co-Doped porous carbon composites for microwave absorption. *Carbon* **2022,** 187, 115-125.
39. Cai, Y.; Cheng, Y.; Wang, Z.; Baoshan, Z., Facile and scalable preparation of ultralight cobalt@graphene aerogel microspheres with strong and wide bandwidth microwave absorption. *Chem. Eng. J.* **2023**, 141102.
40. Wang, B.; Ji, Y.; Mu, C.; Huo, Y.; Xiang, J.; Nie, A.; Xue, T.; Zhai, K.; Liu, Z.; Wen, F., Well-controlled Core-shell structures based on Fe_3O_4 nanospheres coated by polyaniline for highly efficient microwave absorption. *Appl. Surf. Sci.* **2022,** 591.
41. Wang, Q.; Wu, X.; Huang, J.; Siyi Chen; Zhang, Y., Enhanced microwave absorption of biomass carbon/nickel/polypyrrole (C/Ni/PPy) ternary composites through the synergistic effects. *J. Alloy. Compd.* **2021,** 890, 161887.